ChemPubSoc Europe

DOI: 10.1002/celc.201900470

CHEMELECTROCHEM Articles

Comparison of Two Sustainable Counter Electrodes for Energy Storage in the Microbial Rechargeable Battery

Sam D. Molenaar,[a, b] Margo Elzinga,[a] Sonja G. Willemse,[a] Tom Sleutels,[a] Annemiek ter Heijne,*[b] and Cees J. N. Buisman[a, b]

Recently, the microbial rechargeable battery (MRB) has been proposed as a potentially sustainable and low-cost electrical energy storage technology. In the MRB, bioelectrochemical CO_2 reduction and subsequent product oxidation has successfully been combined in one integrated system. However, finding a suitable counter electrode is hindering its further development. In this work, we have tested two alternative counter electrodes in duplicate-namely, i) oxygen/water and ii) a capacitive electrode-for use in the MRB platform. During daily charge/discharge cycling over periods of 11 to 15 days, experimentally obtained energy efficiencies of 25 and 3.7% were reported when using the capacitive and the oxygen/water electrodes, respectively. Large overpotentials, resulting in a voltage efficiency of 15% and oxygen crossover leading to coulombic efficiencies of 25% caused the considerably lower efficiency for the oxygen/water systems, despite the theoretical higher voltage efficiency. Although the capacitive electrode equipped systems performed better, energy density is limited by the operational potential window within which capacitive systems can operate reliably. Microbial community analysis revealed dominant presence of *Geobacter* in the bioanode and *Selenomonadales* in the biocathode. These results do not necessarily bring practical application of the MRB closer, but they do provide new insights in the working principle of this new technology.

1. Introduction

Wind and solar power represent two major alternative energy sources, a possible transition towards renewable energy could be based on.[1] However, wind and solar power are intermittent by nature, and therefore an increasing mismatch between supply and demand of (electrical) energy is foreseen if these renewable sources are to make up for a larger share of the total energy supply. One solution to this mismatch is increasing the use of energy storage technologies. Recently, we demonstrated the use of the microbial rechargeable battery (MRB) as a potential sustainable energy storage technology.[2] The MRB stores electrical energy as chemical energy through the reduction of carbon dioxide to organic metabolites at a biocathode in a process called microbial electrosynthesis (MES).[3–5] During discharge, this chemical energy is converted back into electricity through oxidation of the formed metabolites at a bioanode, while the system functions as a microbial fuel cell (MFC).[6,7]

In order for the MRB to work, the bioanode and biocathode need to be coupled to a counter electrode. This counter electrode needs to possess a sufficiently high potential and reversibility in order to provide substantial cell voltages at useful current densities.[8] In the previously published proof of concept, the ferro/ferricyanide redox couple was used at the counter electrode, as it is known to be highly active and well soluble, operating at an acceptable potential and with low overpotential under the conditions used, without (expensive) catalysts.[2] Integration of this counter electrode into the MRB resulted in overall energy efficiencies of 30 to 40% at an utilized energy density of ~100 Wh/m^3 and discharge power densities of around 190 W/m^3. A disadvantage of using ferro/ferricyanide at the counter electrode is the tendency of the redox couple to form colloidal structures like Prussian blue at the electrode surface, especially in presence of free ferrous iron-ions and at decreased electrolyte mixing, which can impede charge transfer and lead to excessive voltage losses.[9] Therefore, implementation of ferro/ferricyanide into the MRB offers no long-term sustainable solution and alternative counter electrode are needed.

This manuscript explores the use of two alternative counter electrodes for the MRB; (i) a capacitive electrode and (ii) an electrode performing the oxygen/water redox reactions, both of which will be shortly discussed.

In a capacitive electrode, storage or withdrawal of charge (by means of an electrical current) takes place at or from the electrode-electrolyte interface. At this interface, a change in charge density is accompanied by a change in electrostatic double layer (EDL) polarization. As a result of EDL polarization, a

[a] Dr. S. D. Molenaar, M. Elzinga, S. G. Willemse, Dr. T. Sleutels, Prof. C. J. N. Buisman
Wetsus
European Centre of Excellence for Sustainable Water Technology
Oostergoweg 9, 8911 MA Leeuwarden, The Netherlands
[b] Dr. S. D. Molenaar, Dr. A. ter Heijne, Prof. C. J. N. Buisman
Department of Environmental Technology
Wageningen University
Bornse Weilanden 9, 6708 WG Wageningen, The Netherlands
E-mail: annemiek.terheijne@wur.nl

Supporting information for this article is available on the WWW under https://doi.org/10.1002/celc.201900470

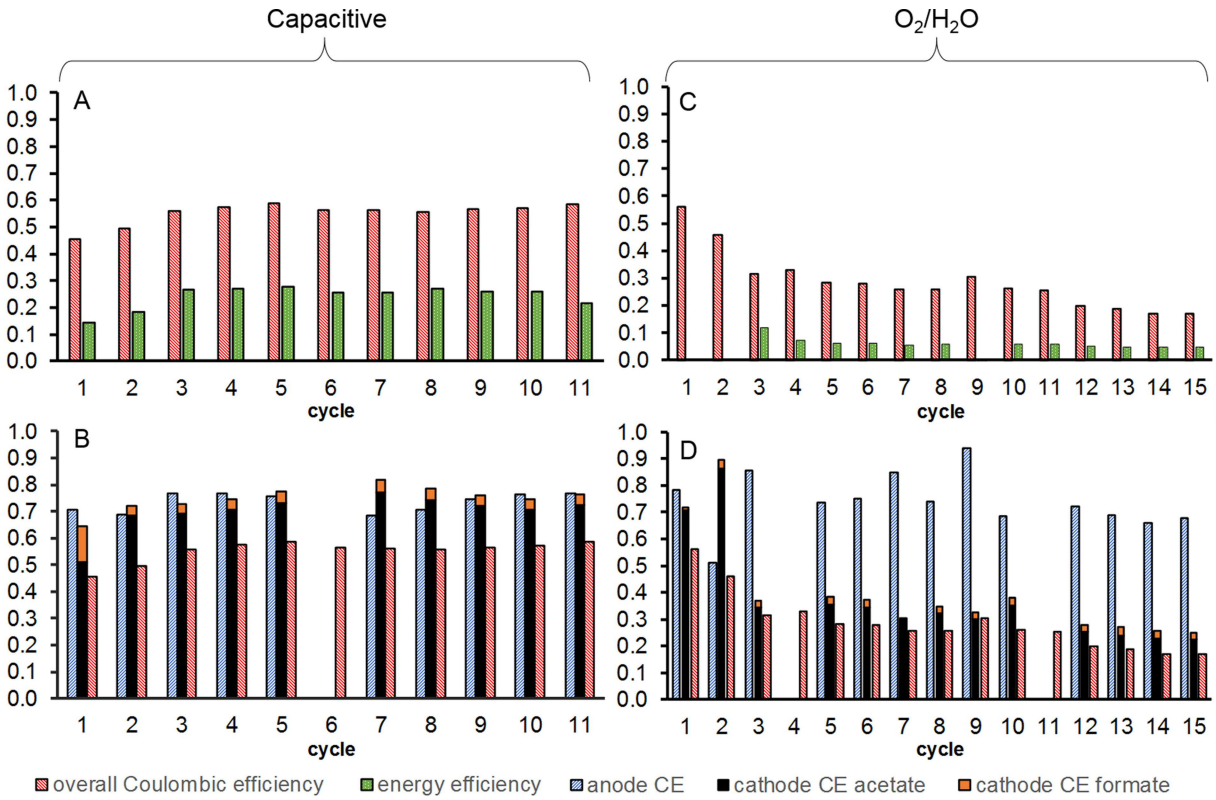

Figure 1. Bar plots of the obtained cycle efficiencies for capacitive (left; A, B) and oxygen/water redox counter electrode equipped (right; C, D) systems. Upper graphs depict the overall energy efficiency and coulombic efficiency, while lower graphs show specific anodic and cathodic coulombic efficiencies, with cathodic efficiency specified per VFA (formate, acetate).

linear relation is obtained between electrode potential and (accumulated) charge, provided ideal capacitive behavior in which no heat is dissipated.[10] The slope of this linear relation, which depends on electrode material, electrolyte composition and physical conditions, represents the capacitance (in Farad, or Coulomb per Volt). As capacitance is an interface property, it scales up (again, linearly) with the surface area of this interface. Thus, a highly porous electrode material, featuring a high specific surface area, generally has a high capacitance.[10] Capacitive electrode materials are specifically designed to feature high specific surface area with a favorable geometry that minimizes mass transfer losses during polarization at higher current densities. The most important advantage of a capacitive electrode – when used properly – is that no faradaic processes take place and as such the energetic losses related to electrochemical reactions can be limited.[11]

When using the oxygen/water redox couple as counter electrode reaction, oxygen is anodically produced during charging of the MRB in the oxygen evolution reaction (OER). During discharging, oxygen is reduced again in the oxygen reduction reaction (ORR). Main advantage of this reaction is the resulting theoretical discharge voltage of 1.11 V, which is significantly higher than the maximum discharge voltage of 0.65–0.7 V obtained when ferricyanide is used.[12,13]

In this manuscript, we have operated two MRBs, one with a capacitive and one with an oxygen/water redox counter electrode during 11 and 15 cycles, respectively. Both MRBs have been operated in duplicate and the performance of these systems has been analysed in terms of power and energy density and Coulombic and voltage efficiency. Finally, also the microbial community of the bioanode and biocathode has been characterized.

2. Results and Discussion

As the results of the duplicate experiments were similar, figures of the results only depict data for a single capacitive and a single O_2/H_2O counter electrode system, allowing comparison between the two types while keeping data presentation comprehensible. Results from the duplicate experiments for both the capacitive and oxygen O_2/H_2O counter electrode are shown in the Supporting Information. Across-cycle Coulombic and energy efficiencies for both systems are presented in Figure 1, while Figure 2 gives a more detailed analysis of the electrochemical charge/discharge behavior in one single cycle.

2.1. Across-Cycle: Coulombic and Energy Efficiencies for Both Counter Electrodes

Prior to the assembly of the MRBs, the pre-cultured bioanodes and biocathodes obtained stable CEs up to 95%. In the initial charging/discharging cycles however, CEs for both biocathodes

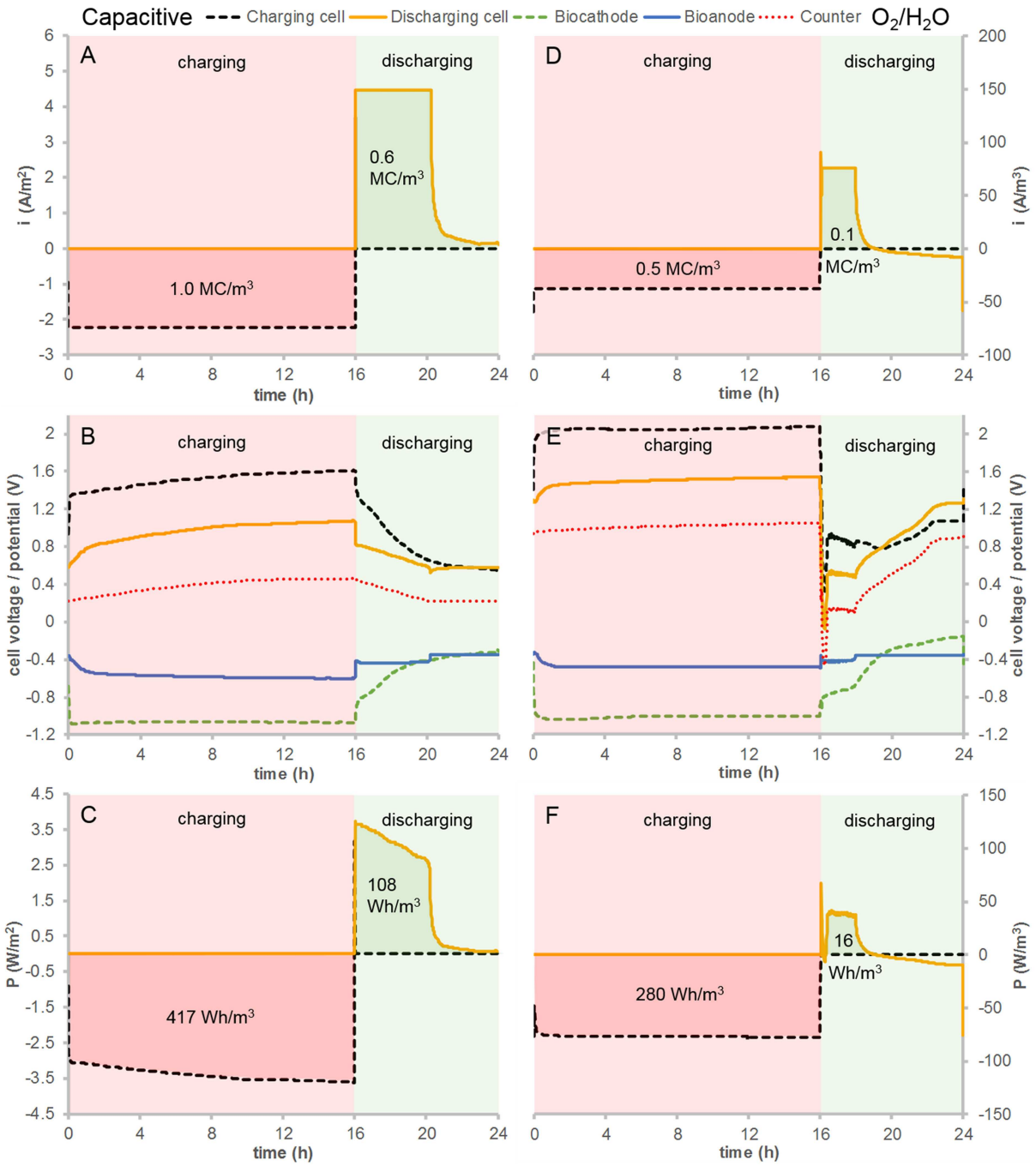

Figure 2. Charging/discharging curves within the 11th cycle of experiments depicting current density, cell voltage, electrode potentials and power density for both systems equipped with a capacitive counter electrode (left, ABC) and oxygen/water counter electrodes (right, DEF).

and bioanodes were considerably lower, between 60% and 80% for both capacitive counter electrode and O_2/H_2O counter electrode experiments (Figure 1A and C). A pronounced difference between the two systems was observed in how CE developed over the cycles that followed. For the MRB with the capacitive counter electrode (Figure 1A), the first two cycles showed relatively low overall CEs (45–50%), progressively leading to higher CEs around 55–60% in subsequent cycles. Combined with VEs of around 40–50% (described in more detail in the following section), this led to energy efficiencies of around 25–28% from the third cycle onwards. Although the CEs in later cycles for these systems were still lower than those observed during pre-culturing of the electrodes, they were comparable with results obtained using ferro/ferricyanide as counter electrode.[2]

For the MRB with the O_2/H_2O counter electrode (Figure 1C), overall CEs dropped steeply during the first cycles, starting at 45–55% in the first two cycles, to stabilize at 17–25% in later

cycles. Due to large overpotentials occurring at this counter electrode during both charge and discharge, overall VEs for these systems were substantially lower (10–20%) than for the capacitive counter electrode and previously tested ferro/ferricyanide counter electrode. Combined with the lower CEs of both bioanode and biocathode, this resulted in overall energy efficiencies of only 2–5%.

Figure 1B depicts a more detailed overview of the CE for the MRB with the capacitive counter electrode, showing for bioanode and biocathode separately. The bioanode of the capacitive electrode started at a CE of 70% in the first cycle to show a slight increase towards 75% by the 11th cycle. The biocathode in this system started at a CE of 65% in the first cycle and increased slightly to 74%. Being very similar, bioanode and biocathode processes contributed almost equally to overall Coulombic losses.

Figure 1D shows the CE for the MRB with the O_2/H_2O counter electrode. The bioanodes of the O_2/H_2O counter electrode equipped systems showed relatively stable CEs ranging between 67 and 90% throughout the cycles and were as such performing similarly to bioanodes in the capacitive systems. The CEs of the biocathode however, while starting at levels of 70–90% in the first two cycles, decreased drastically in the cycles that followed, to 25% in the last cycles.

The main difference between the capacitive and O_2/H_2O counter electrode equipped systems during charging was the presence of oxygen in the counter electrode compartment of the latter. We therefore attribute the low biocathode CE for the O_2/H_2O counter electrode systems to oxygen crossover from the counter electrolyte to the bioelectrolyte.

For the O_2/H_2O counter electrode systems, the biocathode CE (during charging) was three to four times lower than the bioanode CE (during discharging), this despite oxygen concentrations in the counter electrolyte, and thus presumable also oxygen crossover.

Looking more closely at the volatile fatty acids that were produced in the biocathode (Figure 1B and D), in general, the biocathode used the largest fraction of charge to produce acetate for both counter electrodes. However, also a small fraction of formate was detected. Production of formate accounted for 2–3% of the biocathode CE throughout all cycles for the O_2/H_2O counter electrode, while for the capacitive systems 4–10% of cathodic current was directed to production of formate. Production of formate requires a more negative potential compared to reduction towards acetate.[5] Looking at the overall energetics of the MRB this can be beneficial, since the subsequent oxidation reaction at the anode can take place at a more negative potential, leading to a higher cell voltage during discharge. However, formate concentrations as they were detected in current experiments ($\pm$2-5 $mg \cdot L^{-1}$) only played a minor role and as such did not affect overall battery performance substantially.

2.2. Within-Cycle: Electrochemical Charging and Discharging Dynamics

The electrochemical dynamics occurring in a single charging/discharging cycle, showed considerable changes over the initial three cycles for both counter electrodes, after which cycles became more comparable to each other. Figure 2 shows charging/discharging characteristics (current, cell voltage, electrode potentials and power) for both an O_2/H_2O counter electrode and capacitive counter electrode equipped system. These characteristics are based on the 11th cycle, because at this point initial fluctuations had dampened out, and thus can be considered representative for longer-term characteristics.

2.2.1. Charging of the MRB with Capacitive Counter Electrode

Current densities, electrode potentials and cell voltages, and accompanying power densities for the capacitive counter electrode, are shown in Figure 2A, B and C respectively. From these figures it can be concluded that the capacitive counter electrode acted as a nearly ideal capacitor during charging: when the system was controlled at a constant current during the 16 hours of charging, a near-linear increase of the potential of the capacitive counter electrode was observed, starting from around +0.15 V to become +0.45 V at the end of the charging cycle. The fact that electrode potential for the counter electrode showed such a consistent response to exposed current indicates that no undesired redox reaction took take place. Also, the absence of any sudden potential change upon onset of charging indicates that no mass transfer limitations occurred. Regarding the biocathodes, charging resulted in a potential around −1.05 V. This corresponds to the potential at which formation of hydrogen can be expected when graphite is used as an electrode and under the conditions applied here. Overall, an average cell voltage of 1.5 V was required during charging.

During charging the bioanodes were not connected, thus left at OCP, and their potentials slowly decreased from −0.55 V to −0.6 V. With this potential being well below the reversible potential for acetate oxidation, this indicates that the more reductive compounds like hydrogen and formate could also be oxidized by the bioanodes, and that suitable electron transfer mechanisms were in place to do so at a lower electrode potential than used for oxidation of acetate (this in contrast to earlier observations done on hydrogen oxidizing bioanodes as reported by Ntagia et al.[14]).

2.2.2. Discharging of the MRB with Capacitive Counter Electrode

During discharge, bioanodes were operated at constant current at first, leading to an initial anode potential of −0.42 V, which is similar to the potential observed during charging. During this period of constant current, the capacitive counter electrode showed a near-linear decrease in potential. The potential of the capacitive electrode was +0.45 V at the start of the discharge

period and returned closely to its initial potential of +0.15 V. The difference between the bioanode and capacitive counter electrode potential during discharge led to a nominal discharge (cell) voltage of +0.7 V. After a period of relatively constant bioanode potential, substrate started to deplete, upon which bioanode potential rapidly increased to −0.35 V. At this point, the potentiostat switched from current to potential control and bioanodes were controlled at −0.35 V for the remaining time of discharge, as done previously.[2] During this remaining period, a negligible amount of charge was transferred and the potential of the counter electrode remained stable.

Biocathodes were disconnected during discharge. Upon disconnection, biocathode OCP showed a nearly instant increase towards −0.6 V, which corresponds well to the reversible potential for hydrogen/formate oxidation. This initial increase was then followed by a gradual increase towards the bioanode potential, thus nearly reaching −0.35 V at the end of the discharging period. This observation can be explained by the bioanodic processes gradually depleting the electrolyte from reductive compounds, and the biocathode equilibrating well with the overall redox state of the electrolyte.

2.2.3. Charging of the MRB with Oxygen/Water Counter Electrode

The experimental details of the 11th cycle of the O_2/H_2O counter electrode equipped MRB are presented in Figure 2D, E and F. As can be seen in Figure 2D, currents applied in the O_2/H_2O counter electrode were half those as applied to the capacitive counter electrode. This was due to unexpected behavior observed for the O_2/H_2O counter electrode in the first cycle. Polarization curves taken before the actual experiments started, demonstrated that the counter electrode could sustain a discharging current of 5 $A \cdot m^{-2}$ at a potential of 0 V, provided that the oxygen concentration was maintained above 4.4 $mg^{-}L$ (See Supporting information). Neglecting internal resistances in the system, this current density would theoretically result in a positive discharging cell voltage of 0.46 V, with maximum power densities of approximately 5 $W \cdot m^{-2}$. However, during the first cycle's discharge period, the counter electrode potential went down to −0.55 V at a current density of 5 $A \cdot m^{-2}$, at which point the platinized electrode probably started to generate hydrogen. Whether this was caused by a limited availability of oxygen or decreased performance of the used catalyst under the present conditions tested was unknown. Even so, the large overpotentials observed resulted in a slightly negative discharging cell voltage of −0.075 V, and the MRB was thus not functioning as a battery any longer. For this reason, a reduced current of −1.15 $A \cdot m^{-2}$ (charging) and 2.3 $A \cdot m^{-2}$ (discharging) was applied in the following cycles.

Applying these lower currents, Figure 2E shows biocathode potential stabilized at −1 V during the 16 hour charging period. At the same time, the bioanode potential remained at OCP of −0.45 V. This poses a slight difference with the MRBs with capacitive counter electrode, in which bioanode OCP during charging reached lower values of −0.6 V, and may be a direct effect of the presumed oxygen crossover. While charging, the potential of the oxygen redox electrode increased to approximately +1 V. Combined with the biocathode, this overpotential of approximately 0.4 V for the production of oxygen resulted in a cell voltage of 2 V during charging.

2.2.4. Discharging of the MRB with Oxygen/Water Counter Electrode

During the subsequent 8 hour discharging phase, bioanodes were operated at a constant current density of 2.3 $A \cdot m^{-2}$ at a nominal potential of −0.43 V. Anode potentials showed a marked increase in value indicating substrate depletion and therefore anodes were switched from controlled current to control potential at −0.35 V once it reached this point. During discharge, biocathode OCP gradually increased to potentials as high as −0.15 V as oxidizable substrate depleted. This elevated potential strongly indicates the crossover of oxygen to the bioelectrolyte, and this was further strengthened by the observation of small reductive currents for the bioanode after substrate was depleted and potential was controlled.

To provide the counter electrode with sufficient oxygen during discharging, oxygen was supplied to the system during the discharge period. Despite the supply of oxygen starting immediately upon discharging through the action of potentiostat controlled solenoid valves, oxygen concentration in the counter electrolyte still dropped towards 0.4 $mg \cdot L^{-1}$ in the first 7–8 mins of the discharging cycle, after which it increased rapidly to reach a concentration around 7 $mg \cdot L^{-1}$ at the end of the cycle. This initial temporary drop in oxygen was likely caused by a "dead volume" of gas residing in the tubing of the oxygen control system, causing a time delay before oxygen was effectively released into the counter electrolyte. After the initial low oxygen lag phase, stable counter electrode potentials of around 0 V were obtained, resulting in discharging voltages of 0.42 V and power densities up to 1.2 $W \cdot m^{-2}$ (Figure 2B and C). Subsequently, when acetate was fully depleted, a small negative current of −0.2 to −0.3 $A \cdot m^{-2}$ was observed during potential controlled discharging, indicating reduction of crossover oxygen at the bioanode to be dominant at this point. This reductive current at the bioanode resulted in a potential increase of the counter electrode towards +1.05 V, and the energy costs involved were not included in the EE calculation (if these would have been included, it would have led to a reduction of EE of only 0.1 % for the presented cycle, this due to the small current).

Similar to the capacitive counter electrode system, in the O_2/H_2O counter electrode system also considerable overpotentials of 0.54 V were required at the biocathodes to enable hydrogen and consequent acetate production. These overpotentials are commonly observed in biocathodes and may be due to the necessity for hydrogen production as a mediating step for microbial acetate synthesis.[15] The bioanodes operated close to the theoretical potential with observed overpotentials of 0.13 V. The overpotentials of the oxygen redox counter electrode, with a theoretical reversible potential of 0.59 V,

Order	most dominant family/genus within	Bioanode 1	Bioanode 2	Biocathode 1	Biocathode 2	
Bacteroidales	*Rikenellaceae*	5%	7%	4%	12%	Fermentative
Sphingobacteriales	*Lentimicrobium sp.*	4%	1%	4%	2%	
Spirochaetales	*Sphaerochaeta sp.*	1%	2%	1%	2%	
Anaerolineales		2%	0%	1%	0%	
Mollicutes (class)		2%	0%	5%	0%	
Clostridiales	*Proteiniborus sp.*	1%	5%	1%	5%	Homo-acetogenic
Selenomonadales	*Sporomusa sp.*	12%	11%	31%	30%	
Pseudomonadales	*Thiopseudomonas sp.*	3%	1%	10%	6%	H_2/CO/formate-based EET
Burkholderiales	*Hydrogenophaga sp.*	0%	0%	1%	1%	
Rhodocyclales	*Dechlorobacter sp.*	17%	23%	21%	23%	
Desulfovibrionales	*Desulfovibrio sp.*	1%	2%	3%	5%	Cytochrome based EET
Desulfuromonadales	*Geobacter sp.*	43%	39%	8%	4%	
Other		7%	5%	8%	8%	
Unidentified		2%	2%	2%	2%	

Figure 3. Heat map showing relative abundance of taxonomic assignments of OTUs at the order level as resulted from the 16 S rRNA sequencing of samples of both bioanodes and biocathodes of the capacitive electrode equipped systems. Results for both duplicates are shown (bioanode/biocathode 1&2). For the full taxonomic assignment results, see the Supporting Information. Provisional functional grouping, depicted on the right, was suggested based on previous reports on mentioned groups and references to these reports are provided in the text.

amounted to approximately 0.41 V during charging and 0.59 V during discharging.

2.3. Microbial Community Diversity

Figure 3 shows a heat map of the 16 S rRNA gene sequencing results with the relative abundance of the taxonomic assignments at the order level. All assigned reads with an abundance greater than 1% are displayed separately. In case additional taxonomic assignments of OTUs at the family/genus level showed a high abundance of one or few taxonomic groups within an order, these are mentioned in Figure 3 as well.

Overall, Figure 3 shows a clear distinction between bioanodes and biocathodes. Most characteristic for the bioanodes is the dominant occurrence of *Geobacter* species, as is to be expected and well described previously for these systems.[16,17] Together with species belonging to *Desulfovibrionales*, direct extracellular electron transfer (EET) from or to an electrode by means of membrane bound cytochromes has been demonstrated for this group of bacteria,[18,19] and their high relative abundance specifically on the bioanode matches with the relatively low overpotentials observed there during discharge of the MRB.

The cathode in turn shows, as most prominent species, those belonging to the *Selenomonadales* order. Most dominantly represented within this order are species belonging to the genus *Sporomusa,* which have been previously investigated for their role in acetate producing biocathodes.[15,20] Together with bacteria within the (here less abundant) order of *Clostridiales, Selenomonadales* comprise a group within which numerous homoacetogenic species reside, and most of the species within these orders are capable of performing the Wood-Ljungdahl pathway for producing acetate from CO_2 and H_2.[20] The clear difference in abundance for *Selenomonadales* between bioanodes and biocathodes found here underpins this role.

On the second place in relative abundance, for both bioanodes and biocathodes, are species belonging to the order of *Rhodocyclales*, with most OTUs assigned to the genus *Dechlorobacter*. These have been reported frequently in biocathodes, but are found in higher relative abundance in bidirectional bioelectrodes, initially operated as anodes before being poised more negative potentiall.[21–23] Species belonging to the orders of *Pseudomonales* and *Burkholderiales,* have been described as co-occurring under these conditions, and may play a comparable role.[21,23] The association of these groups of bacteria specifically with reversed electrodes seems to provide, although not fully, a basis for constructing a bi-directional bioelectrode, in which the biota present can gain energy both by electrogenic oxidation and electrotrophic reduction. If successfully established, this could reduce the MRBs footprint by integration of bioanode and biocathode. Supportive to this hypothesis is the recent report of such an bi-directional electrode by Yates *et al.*,[24] in which growth of electrocatalytic biomass was established by inversion of polarity on a 10 min interval. It would be interesting to investigate whether this functionality can be maintained over longer charge/discharge intervals.

2.4. Comparison of the Counter Electrodes Tested So Far: Implications and Future Perspective

Table 1 shows a comparative overview of the obtained and theoretical maximally attainable key parameters for the MRB with

the three by now tested counter electrodes. Quantities are given regarding Coulombic, voltage and energy efficiency, and energy and power densities. Experimentally obtained numbers are taken from existing and presented datasets. For the estimation of theoretical maxima, the following assumptions were made: (1) an achievable volumetric current density of 750 $A \cdot m^{-3}$ for all biocatalyzed electrodes at which (2) acetate producing biocathodes are able to be operated at a potential of −0.87 V,[25] (3) acetate oxidizing bioanodes to be operated at −0.42 V,[26] (4) capacitive counter electrodes both during charging and discharging to be operated at a nominal potential of 0.15 V, assuming an operational potential window of 0.6 to −0.3 V, (5) biocatalyzed oxygen reduction at a potential of 0.3 V[27] (6) anodic oxygen evolution at a potential of 1 V and (7) gaseous oxygen being stored at a molar density of 0.01 $mol \cdot m^{-3}$. Coulombic losses are assumed to be limited to 20% for all types of counter electrode, assuming oxygen crossover to be less problematic once current densities are increased. Charge storage was assumed to take place in the form of acetate, with maximum attainable concentrations of 0.75 M[28], and in case of ferro/ferricyanide as a counter electrode redox couple, a maximum solubility of 1 M was used. Finally, for the power density maximum projections, ferro/ferricyanide and capacitive electrodes were assumed to be non-limiting with regard to current density, thus with only the volume of biologically catalyzed electrodes defining attainable power density. Furthermore, no operational energy losses were taken into account.

Looking at Table 1, it is clear that the capacitive counter electrode equipped systems outperformed the MRBs with an O_2/H_2O counter electrode on all aspects in the current experiments. However, using capacitive electrodes in aqueous environments limits the attainable energy density: restricted in potential window by electrolysis of water, during charging the capacitive electrode potential may not increase much further than +0.7 V, after which oxygen production (and concomitant oxidation of the carbon compounds) may occur, thus not contributing any longer to double layer polarization. When discharging, the capacitive electrode potential may not decrease to values too close to the anode potential (−0.4 V in these experiments) in order to maintain meaningful discharge cell voltages. As such, a theoretical voltage window of 1.1 V is available to the capacitive electrode which allows for only limited charge densities given the currently obtained capacities around 65 $F \cdot g^{-1}$ (dry weight).

With the O_2/H_2O counter electrode, MRB performance is severely limited by the combined effects of both oxygen crossover, affecting the CE, and the slow reaction kinetics of both the ORR and OER. Especially the large overpotential currently required for ORR is problematic, as this limits the obtainable current and power density during discharging. The relative impact of oxygen crossover on CE may be substantially lowered in case a faster ORR can be established without increasing oxygen concentrations, as the flux of oxygen crossover only depends on concentration gradient, and not on current. A possible future implementation and optimization of biologically catalysed oxygen reduction into the MRB platform might provide possibilities to this extent; with specific current densities of 0.9 $A \cdot m^{-2}$ reported for flat graphite plate cathodes polarized at 0.15 V.[27] When adequately operated on a three-dimensional electrode material, sufficiently high volumetric current densities should be feasible at oxygen concentrations comparable to those used in current experiments. However, this would still not dispel the requirements of precious catalysts for the anode reaction, severely impeding the economic and ecological principles this battery strives for.

Table 1. Comparison of the so-far-tested counter electrodes with use in the MRB. Both experimentally acquired values (exp., left numbers) as projected theoretical maximum attainable values (max., right numbers) are displayed.

	Ferro/ferricyanide		Capacitive		O_2/H_2O	
	exp.	max.	exp.	max.	exp.	max.
Coulombic efficiency [%]	65	80	55	80	25	80
Voltage efficiency [%]	54	63	45	58	15	44
Energy efficiency [%]	35	50	25	45	3.7	35
Energy density [$W \cdot h \cdot L^{-1}$]	0.1	17	0.1	2.5	0.02	82
Power density [$W \cdot L^{-1}$]	0.2	58	0.1	43	0.04	31

The capacitive electrode has proven to be a stable counter electrode in the microbial rechargeable battery. Losses encountered can be mainly attributed to the performance of the biocathode, with lower cycling efficiency compared to the use of ferro/ferricyanide being caused by the biocathodes' overpotential having a relatively larger impact on VE given the slightly lower nominal potential of the capacitive electrode. A reduction in overpotential at the biocathode could improve performance at this point. This is however not foreseen as both from our own experiments and other work[15] it seems that hydrogen is an inevitable mediating compound in the reduction of CO_2 towards carboxylates in BESs at relevant current densities.

3. Conclusions

Although by the data presented in the current study the capacitive system is outperforming the oxygen reduction reaction equipped MRBs in terms of energy efficiency by a factor of 5, the potential upscaling in terms of energy density is foreseen to be problematic due to relatively low charge capacity associated with EDL charging. With this regard, the use of the O_2/H_2O electrode may provide a more optimistic outlook, with theoretically attainable energy densities of around 82 $Wh \cdot L^{-1}$ and a cycling efficiency of up to 38%, under the mentioned assumptions. However also for the H_2O/O_2 electrode, inevitable disadvantages remain, most notably the requirement of precious metal catalysts for performing the OER and the need for oxygen produced during charging to be stored under high pressures, with safety issues and energy losses associated. Although these results do not necessarily bring practical application of the MRB closer, they do provide new insights in the working principle of this new technology.

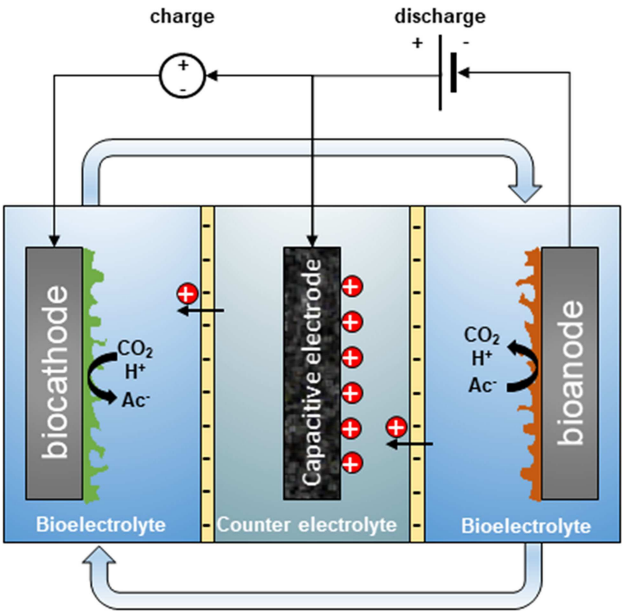

Figure 4. Schematic drawing of the MRB equipped with a capacitive counter electrode. The counter electrode was sandwiched between the biocathode (left) and bioanode (right), which was hydraulically separated from the bioelectrolyte by two cation exchange membranes (yellow). Bioelectrolyte was recirculated over the two bioelectrode compartments. When charging, a current was applied between biocathode and capacitive electrode, while at discharging a controlled current from bioanode to capacitive electrode was maintained at a level to deliver a positive cell voltage.

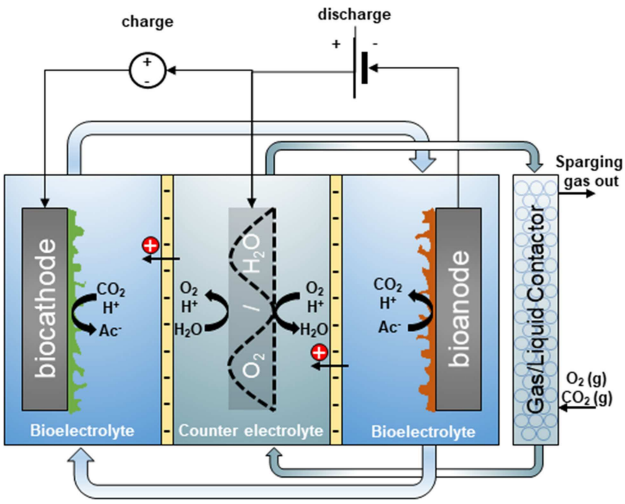

Figure 5. Schematic drawing of the MRB equipped with an O_2/H_2O counter electrode. The curved dashed line in the middle compartment represents the Pt/IrO_2 catalyzed titanium mesh that was shaped to fill the counter electrode compartment while supporting the two cation exchange membranes (yellow). The counter electrolyte was recirculated over the gas/liquid contactor depicted on the right, where O_2 and CO_2 were added by mass flow controllers. Bioelectrolyte was recirculated over the two bioelectrode compartments. When charging, a current was applied between biocathode and capacitive electrode, while at discharging a controlled current from bioanode to capacitive electrode was maintained at a level to deliver a positive cell voltage.

Experimental Section

General MRB Design

Two MRB systems were constructed for each type of counter electrode, i.e. testing each type in duplicate. A schematic overview of the constructed systems, one with the capacitive and one with the O_2/H_2O redox counter electrode, are visualized in Figure 4 and Figure 5. For both systems, the counter electrode was placed in between the biocathode and bioanode, and the compartments were separated by a cation exchange membrane (projected surface area of 22 cm^2, Nafion® 117). The bioanodes and biocathodes both consisted of graphite felt (3 mm, FMI Composites Ltd., Galashiels, Scotland), in which electro-active biofilms were pre-grown (see section 'microbial inoculum'). Five layers of graphite felt were used for each electrode, filling the flow compartments completely (inner dimensions 110×20×15 mm, 33 cm^3). As current collector for both biocathode and bioanode, a layer of graphite paper was placed on a solid stainless-steel plate (SS316). The felt was firmly pressed against the graphite paper/stainless steel assembly once systems were closed, assuring proper electrical contact.

The electrolyte, shared between bioanode and biocathode (further referred to as bioelectrolyte), was continuously recirculated between the biocathode and bioanode flow compartments by a peristaltic pump (Masterflex, Canada). O-rings and silicon gaskets sealed the stacked elements and the entire cell was closed with rubber-coated bolts.

The temperature of the systems was controlled at 30±2 °C at all times. Potentials of all electrodes were measured and reported against reference electrodes (Ag/AgCl, Prosens, Oosterhout, The Netherlands; +0.203 V vs SHE) and galvanically connected to the electrolytes adjacent to the electrodes using a Haber-Luggin capillary filled with 3 M KCl. All cell voltages and electrode potentials were monitored and data were collected with a data logger (RSG40, Endress+Hauser, Reinach, Switzerland). The pH of the bioelectrolyte was measured in-line (CP571D-7BV21, Endress+Hauser, Gerlingen, Germany). Any gas production at the bioelectrodes was monitored with a gas bubble counter (MGC, Ritter Apparatebau, Bochum, Germany). All electrochemical methods were applied and recorded with a potentiostat (N-stat DC, Ivium Technologies, Eindhoven, The Netherlands).

Capacitive Counter Electrode

The capacitive counter electrode consisted of a flow compartment completely filled with activated carbon granules (Norit® PK 1–3, from peat, steam activated). Two titanium mesh electrodes (2 mm thickness) were used as current collectors, one at each side of the capacitive electrode, firmly contacting the granules while allowing ionic conductivity towards both bioanode and biocathode. Prior to use, granules were soaked in the to-be-used electrolyte and degassed for 1 hour. The electrolyte in the capacitive flow chamber was recirculated continuously over a small glass compartment positioned above the flow compartment, thus allowing any produced gases to leave the electrolyte and guaranteeing the granules to be gas-free at all times. Prior to use in the MRB, the capacitive granules were weighed and capacitance was determined in multiple charge/discharge cycles (see Supporting Information). Within the tested potential range, a capacitance of 481 Farad was determined, based on a specific capacity of 65 $F \cdot g^{-1}$ (dry weight) and a weight per electrode of 7.4 g.

Oxygen/Water Counter Electrode

The bi-directional oxygen reduction and water oxidation counter electrode (further referred to as the O_2/H_2O counter electrode) consisted of a Pt:IrO_2 coated titanium mesh which was shaped to fill the counter electrode compartment and keep the bioanode and biocathode in place. The counter electrolyte was continuously recirculated over a glass column filled with glass beads (4 mm diameter), serving as gas/liquid contactor. Mass flow controllers were set to continuously sparge the counter electrolyte with 2.5 $mL \cdot min^{-1}$ CO_2 at an inlet situated at the bottom of the column. Additional relay-actuated mass flow controllers provided a co-flow of pure oxygen (0.6 $mL \cdot min^{-1}$) during the periods when cells discharged. The oxygen concentration in the counter electrolyte was measured in-line using an amperometric oxygen probe (Endress + Hauser, Oxymax COS22D, Gerlingen, Germany) placed between the electrode flow compartment and the gas/liquid contactor.

Media Composition

The bioelectrolyte consisted of 0.4 $g \cdot L^{-1}$ NH_4HCO_3, 0.05 $g \cdot L^{-1}$ Ca$(OH)_2$, 0.1 $g \cdot L^{-1}$ $MgSO_4$ $7H_2O$, 9.6 $g \cdot L^{-1}$ K_2HPO_4, 2.1 $g \cdot L^{-1}$ Sodium 2-bromoethanesulfonate (Na-2-BES), 4.0 $g \cdot L^{-1}$ NaOH, 0.1 $mL \cdot L^{-1}$ trace metals, and 0.1 $mL \cdot L^{-1}$ vitamins (DSMZ medium 141).[29] Before use, the solution was saturated with CO_2, with a resulting pH of 7. The electrolyte used at the capacitive counter electrode was identical in composition to the bioelectrolyte solution, with as exceptions that Na-2-BES, trace metals and vitamins were omitted. Electrolyte used at the O_2/H_2O counter electrode consisted of a CO_2 saturated 100 mM potassium-phosphate solution buffering at pH 7. All electrolytes were recirculated at 50 $mL \cdot min^{-1}$.

MRB Inoculum

Individual biocathodes were started 3 and bioanodes 2 weeks prior to assembly of the MRBs. These biocathode and bioanode cells were assembled and operated as described earlier for the MRB.[2] Both biocathodes and bioanodes were continuously fed with fresh bioelectrolyte at 0.125 $mL \cdot min^{-1}$. For the bioanode, the bioelectrolyte was complemented with 10 mM sodium acetate. Bioanodes were controlled at a potential of −0.35 V while the biocathodes were initially controlled at a current of $-4.55\ A \cdot m^{-2}$ for 4 days and then changed to a current density of $-9.09\ A \cdot m^{-2}$. 1 mL of a 50 vol% mixture of anaerobic sludge from the municipal wastewater treatment plant in Leeuwarden and cow manure was used as inoculum for the biocathodes and 5–20 mg (wet weight) biomass from previously operated acetate-oxidizing anodes was used to inoculate the anodes. Daily measurements of the VFA concentrations in the bioelectrolyte were performed in the week before the electrodes were inoculated in the MRB to confirm efficient production of acetate for the biocathodes. Prior to the assembly of the MRBs, these pre-cultured bioanodes and biocathodes obtained stable Coulombic efficiencies (CE) up to 95%, and biocathodes converted electrons to acetate at potentials between −0.9 V and −1.1 V. To assemble the MRBs, the biocathode and bioanode systems were dissembled and bioelectrodes were transferred to the MRBs.

MRB Start-up and Operation

Directly after transferring the bioelectrodes, the MRBs were filled with electrolyte and recirculation was started to remove air. Before the actual testing of the MRB was started, systems were alternately charged/discharged every 30 minutes as a pre-treatment, for 5 consecutive days. During this pre-treatment period, biocathodes were current-controlled at $-2.27\ A \cdot m^{-2}$ during the charging period, while the anode was at OCP. During the subsequent discharging period, anodes were current-controlled at $4.55\ A \cdot m^{-2}$ and biocathodes were at OCP. In case the anode potential increased to values higher than −350 mV, the potentiostat switched to control the potential at this value, this to avoid undesired oxidative processes when acetate was depleted. A small continuous flow of 0.06 $mL \cdot min^{-1}$ of fresh bioelectrolyte was fed to the systems to assure sufficient macronutrients and inorganic carbon for a good recovery of both bioanodic and biocathodic functions. Additionally, for the capacitive counter electrodes, Coulombic losses occurring throughout charging/discharging led to asymmetric currents, with the overall electrode potential steadily increasing over time. Thus, in the last day of pre-treatment, a dose of acetic acid was added to the bioanode to bring down the potential of the capacitive electrodes to a potential of approximately 0 V at the end of the last discharge cycle.

Timing for charging and discharging was set to 16 and 8 hours to mimic a day-night rhythm. As it turned out after the first cycle, the O_2/H_2O counter electrodes could not sustain reductive currents of $4.55\ A \cdot m^{-2}$ at sufficiently low overpotential, yielding negative discharge cell voltages (for more details see Results and Discussion). For this reason, a lower current of $-1.15\ A \cdot m^{-2}$ (charge) and $2.3\ A \cdot m^{-2}$ (discharge) was applied to these systems in the following cycles.

System performance was monitored in detail during 11 cycles for the capacitive counter electrode, and 15 cycles for the O_2/H_2O counter electrode. After these cycles, the behavior of both systems did not change considerably, and experiments were ended. In case of the capacitive systems, bioelectrodes were harvested for microbial community analysis.

Microbial Community Analysis

Samples for microbial community analysis were taken from the systems equipped with capacitive counter electrodes after the experiment had been completed. Bioelectrodes were taken out of the assembly, put in 50 mL tubes, snap-frozen in liquid nitrogen and stored at −80 degrees until further processed. Bacterial/archaeal community analysis of these samples was performed using high-throughput 16 S rRNA gene sequencing in order to obtain relative abundances for taxonomic assignments to Operational Taxonomic Units (OTUs). Details on the materials and methods for DNA extraction and microbial community analysis are reported in the Supporting Information.

Chemical Analysis and Calculations

Current and power densities are normalized to both projected membrane surface area (22 cm^2) and bioelectrode volume (33 cm^3). Energy and charge densities were normalized to bioelectrolyte recirculation volume (300 mL) to allow comparison with previously studied setups.

To determine the individual CE of the anode and cathode, the bioelectrolyte was sampled 15 minutes before the end of each charge and discharge period. The sampling volume, 1 mL, was replaced with an equal amount of CO_2 saturated medium. Samples were analyzed for VFA content using a Dionex UHPLC system equipped with a Phenomenex Rezex Organic Acid H+ 300× 7.8 mm column, with a lower detection limit for formate and acetate of 0.5 $mg \cdot L^{-1}$ and 1 $mg \cdot L^{-1}$ for subsequent VFAs (propionate, butyrate etc.) CE for the anode, cathode and for the total system were calculated according to Equations (1)–(3):

$$CE_{an} = \frac{\int_{16}^{24} I\,dt}{\Delta c_{VFA} \cdot V \cdot n \cdot F} \quad (1)$$

$$CE_{cat} = \frac{\Delta c_{VFA} \cdot V \cdot n \cdot F}{\int_{0}^{16} I\,dt} \quad (2)$$

$$CE_{total} = \frac{\int_{16}^{24} I\,dt}{\int_{0}^{16} I\,dt} \quad (3)$$

Where I is the current (A), Δc_{VFA} is the concentration change in volatile fatty acids over the measured time interval ($mol \cdot L^{-1}$, separate calculations were made in case multiple VFAs were detected), V is the total recirculation volume (300 mL), n the number of electrons involved in the oxidation or reduction reaction (8 for acetate, 2 for formate, 12 for succinate) and F is the Faraday constant (96485 $C \cdot mol^{-1}$).

The overall energy efficiency (EE; %) was calculated according to Equation (4):

$$EE = \frac{\int_{16}^{24} P\,dt}{\int_{0}^{16} P\,dt} \quad (4)$$

Where P is the electrical power applied/obtained during charging/discharging (W). The nominal voltage efficiency (VE) was defined as ratio between the overall energy efficiency and the CE [Eq. (5)]:

$$VE = \frac{EE}{CE} \quad (5)$$

Acknowledgements

This work was performed in the cooperation framework of Wetsus, European Centre of Excellence for Sustainable Water Technology (www.wetsus.eu). Wetsus is co-funded by the Dutch Ministry of Economic Affairs and Ministry of Infrastructure and Environment, the Province of Fryslân, and the Northern Netherlands Provinces. The authors like to thank the participants of the Resource Recovery research theme for the fruitful discussions and their financial support.

Conflict of Interest

The authors declare no conflict of interest.

Keywords: bioelectrochemical systems · microbial electrosynthesis · energy storage · microbial rechargeable batteries · microbial electrochemical technology

Manuscript received: March 20, 2019
Revised manuscript received: March 20, 2019
Accepted manuscript online: April 9, 2019

[1] K. E. Trenberth, J. T. Fasullo, J. J. Kiehl, *Bull. Am. Meteorol. Soc.* **2009**, *90*, 311–323.
[2] S. D. Molenaar, A. R. Mol, T. H. J. A. Sleutels, A. Ter Heijne, C. J. N. Buisman, *Environ. Sci. Technol. Lett.* **2016**, *3*, 144–149.
[3] K. Rabaey, R. A. Rozendal, *Nat. Rev. Microbiol.* **2010**, *8*, 706–716.
[4] L. Jourdin, T. Grieger, J. Monetti, V. Flexer, S. Freguia, Y. Lu, J. Chen, M. Romano, G. G. Wallace, J. Keller, *Environ. Sci. Technol.* **2015**, *49*, 13566–13574.
[5] S. D. Molenaar, P. Saha, A. R. Mol, T. H. J. A. Sleutels, A. ter Heijne, C. J. N. Buisman, *Int. J. Mol. Sci.* **2017**, *18*, 204.
[6] B. E. Logan, B. Hamelers, R. Rozendal, U. Schröder, J. Keller, S. Freguia, P. Aelterman, W. Verstraete, K. Rabaey, *Environ. Sci. Technol.* **2006**, *40*, 5181–5192.
[7] T. Sleutels, S. Molenaar, A. Heijne, C. Buisman, *Microorganisms* **2016**, *4*, 7.
[8] X. Luo, J. Wang, M. Dooner, J. Clarke, *Appl. Energy* **2015**, *137*, 511–536.
[9] C. M. Pharr, P. R. Griffiths, *Anal. Chem.* **1997**, *69*, 4673–4679.
[10] H. Kelly-Holmes, *Advert. as Multiling. Commun.* **2016**, *45*, 1–206.
[11] S. Porada, R. Zhao, A. Van Der Wal, V. Presser, P. M. Biesheuvel, *Prog. Mater. Sci.* **2013**, *58*, 1388–1442.
[12] V. Shahrezaei, P. S. Swain, *Proc. Mont. Acad. Sci.* **2008**, *105*, 17256–17261.
[13] J. E. O'Reilly, *BBA-Bioenerg.* **1973**, *292*, 509–515.
[14] E. Ntagia, P. Rodenas, A. Ter Heijne, C. J. N. Buisman, T. H. J. A. Sleutels, *Int. J. Hydrogen Energy* **2016**, *41*, 5758–5764.
[15] H. D. May, P. J. Evans, E. V. LaBelle, *Curr. Opin. Biotechnol.* **2016**, *42*, 225–233.
[16] F. Kracke, I. Vassilev, J. O. Kr??mer, *Front. Microbiol.* **2015**, *6*, 1–18.
[17] R. Kumar, L. Singh, Z. A. Wahid, M. F. M. Din, *Int. J. Energy Res.* **2015**, *39*, 1048–1067.
[18] C. S. Kang, N. Eaktasang, D. Y. Kwon, H. S. Kim, *Bioresour. Technol.* **2014**, *165*, 27–30.
[19] D. R. Lovley, *Environ. Microbiol. Rep.* **2011**, *3*, 27–35.
[20] K. P. Nevin, S. A. Hensley, A. E. Franks, Z. M. Summers, J. Ou, T. L. Woodard, O. L. Snoeyenbos-West, D. R. Lovley, *Appl. Environ. Microbiol.* **2011**, *77*, 2882–2886.
[21] R. Mateos, A. Sotres, R. M. Alonso, A. Escapa, A. Morán, *Bioelectrochemistry* **2018**, *121*, 27–37.
[22] H. Yun, B. Liang, D. Kong, A. Wang, *Chemosphere* **2018**, *194*, 553–561.
[23] L. Jourdin, Y. Lu, V. Flexer, J. Keller, S. Freguia, *ChemElectroChem* **2016**, *3*, 581–591.
[24] M. D. Yates, L. Ma, J. Sack, J. P. Golden, S. M. Strycharz-Glaven, S. R. Yates, L. M. Tender, *Environ. Sci. Technol. Lett.* **2017**, *4*, 374–379.
[25] L. Jourdin, S. Freguia, V. Flexer, J. Keller, *Environ. Sci. Technol.* **2016**, *50*, 1982–1989.
[26] K. Guo, D. Hidalgo, T. Tommasi, K. Rabaey, *Bioresour. Technol.* **2016**, *211*, 664–668.
[27] M. Rothballer, M. Picot, T. Sieper, J. B. A. Arends, M. Schmid, A. Hartmann, N. Boon, C. J. N. Buisman, F. Barrière, D. P. B. T. B. Strik, *Bioelectrochemistry* **2015**, *106*, 167–176.
[28] M. Demler, D. Weuster-Botz, *Biotechnol. Bioeng.* **2011**, *108*, 470–474.
[29] A. J. B. Zehnder, B. A. Huser, T. D. Brock, K. Wuhrmann, *Arch. Microbiol.* **1980**, *124*, 1–11.